ORIGINAL ARTICLE

Study on the Influence of Magnetic Circuit Saturation on Suspension Performance of Bearingless Permanent Magnet Synchronous Motor

Liming Liu[1] · Hongbo Qiu[1]

Abstract

Bearingless permanent magnet synchronous motors can rely on the radial electromagnetic force generated by magnetic field coupling to achieve active suspension. However, the coupling between magnetic fields may lead to the saturation of the magnetic circuit, which affects the stability of motor suspension force and is one of the key problems to be solved for bearingless motors. In order to investigate the effect of magnetic circuit saturation on the suspension performance, firstly, the equation of the radial suspension force is derived by combining the influence of the magnetic circuit saturation on the parameters of the motor. The relationship of the magnetic circuit saturation on the stable and fluctuating components of the radial suspension force is obtained, and the fluctuation mechanism of the suspension force under the saturation state is revealed. Secondly, the radial suspension force in different saturation states of the magnetic circuit is calculated by finite element calculation method. Combining the effect of magnetic flux density on the magnetic permeability, the variation of the magnitude and fluctuating of the suspension force with the magnetic field in different magnetic circuit saturation states is given. Finally, the accuracy of the analytical and finite element calculations is demonstrated experimentally.

Keywords Bearingless permanent magnet synchronous motor · Magnetic field distribution · Magnetic circuit saturation · Suspension force stability

1 Introduction

The bearingless permanent magnet synchronous motor integrates the functions of conventional permanent magnet synchronous motor and magnetic bearing, which not only has the advantages of frictionless magnetic bearing, no lubrication and long life, but also achieves high integration and system simplification [1–3].Therefore, bearingless permanent magnet synchronous motors have potential applications in some special fields, such as high-speed precision electric spindles, flywheel energy storage, blood pumps and centrifugal pumps [4–8].

For the problem of magnetic circuit saturation, many scholars have conducted a series of studies and verifications.

Literature [9] proposed a load field prediction model of double-winding permanent magnet synchronous motor based on subdomain model and combined with the equivalent magnetic circuit method to compensate the magnetic saturation of the iron core, which effectively improved the compensation accuracy and made the motor control model more accurate. Based on the basis formula of torque and suspension and combined with gap permeability theory. Literature [10] analyzed the effect of magnetic saturation on edge flux. The radial force and torque from linear region to saturated region are calculated effectively, which provides theoretical support for the stable operation of bearingless switched reluctance motor under full torque load. Literature [11] proposed a mathematical model considering magnetic saturation and carried out a regional analysis according to the electromagnetic saturation effect. Based on the influence of different parameters on the motor performance, the motor control strategy is improved, which has certain reference value for the optimization design and control performance. In order to characterize the phenomenon of local magnetic saturation in the process of rotor rotation. Literature [12] introduced a modified coefficient of rotor

✉ Liming Liu
   332101050090@email.zzuli.edu.com

   Hongbo Qiu
   liuliminglli@163.com

[1] School of Electric and Information Engineering, College of Electrical and Information Engineering, Zhengzhou University of Light Industry, Zhengzhou, Henan, China

yoke permeability, which greatly shortened the calculation time of finite element analysis and greatly improved the efficiency of machine design. Literature [13] proposed an analytical model of torque considering magnetic saturation and completed the nonlinear torque model through B-H loop. According to finite element calculation, the effectiveness of the proposed modelling method was verified. Literature [14] uses a combination of the response surface model and a multi-objective optimization algorithm to optimize the suspension stability and torque. The optimization process considers not only geometric parameters but also winding distribution. Literature [15] linearizes the mathematical model of BPMSM to achieve optimal control, considering coupling and nonlinearity issues.

Existing analytical methods for bearingless motors mainly focus on the optimization of control algorithms. In this paper, the influence of magnetic circuit saturation on bearingless motor performance is studied from the aspect of electromagnetic calculation and analysis, on the basis of magnetic circuit coupling analysis, the nonlinear variation law of radial suspension force under different magnetic circuit saturation is determined by establishing the radial suspension force nonlinear mathematical model, and the influence mechanism of magnetic circuit saturation on the stable component and fluctuation component of radial suspension force is revealed.

Firstly, the working mechanism of the bearingless permanent magnet synchronous motor is analyzed, and based on the magnetic circuit method, the effect of magnetic circuit saturation on the motor parameters is revealed. Secondly, based on the traditional suspension force formula, the suspension force analytical model considering the magnetic circuit saturation is derived, the variation of suspension force under different saturation conditions of magnetic circuit is determine, and the principle of suspension force fluctuation under saturation condition is revealed. In addition, the radial suspension force under different magnetic circuit saturation states is calculated by finite element method, and the results consistent between the analytical analyses and the finite element calculations are determined. Finally, the accuracy of the analytical and finite element calculations is demonstrated by experiments.

2 Working Mechanism and Magnetic Circuits of Bearingless Permanent Magnet Synchronous Motor

The stator of bearingless permanent magnet synchronous motors is embedded with suspension winding and torque winding with different pole pairs. The coupling of the magnetic fields of suspension and torque changes the symmetric distribution of magnetic field, so that the motor can provide
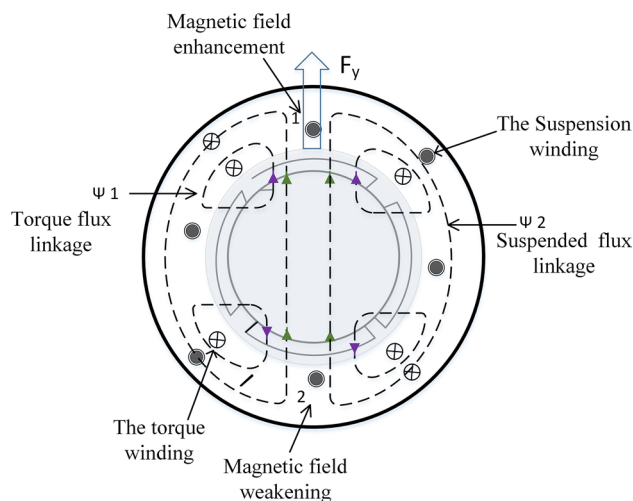
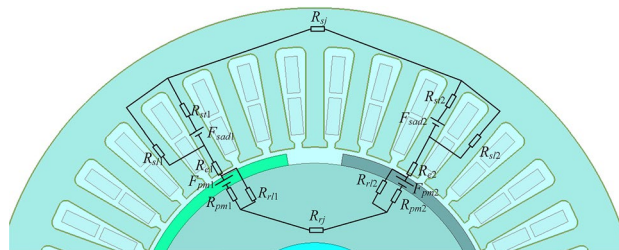**Fig. 1** Working principle of bearingless permanent magnet synchronous motor

Fig. 2 The magnetic circuit of a permanent magnet synchronous motor

torque and generate the suspension force to support the rotor suspension. Figure 1 shows the working principle of the bearingless permanent magnet synchronous motor.

The Fig. 1 gives the distribution of the 4-pole flux linkage Ψ1 generated by the torque magnetic field and the 2-pole flux linkage Ψ2 generated by the suspension magnetic field. In the motor, the flux linkage Ψ1 and Ψ2 are enhanced in the same direction and weakened in the opposite direction, which cause the asymmetric distribution of magnetic field. According to maxwell force generation principle, a radial electromagnetic force along the direction of magnetic field enhancement will be generated. By controlling the magnitude and phase of the current flowing into the suspension winding, the magnitude and direction of suspension force can be regulated, which achieve the stable suspension of rotor. Due to the asymmetric distribution of magnetic field, the part of magnetic flux density enhancement is easy saturation, which affects the suspension force stability. Figures 2 and 3 shows the magnetic circuit of the permanent magnet motor.
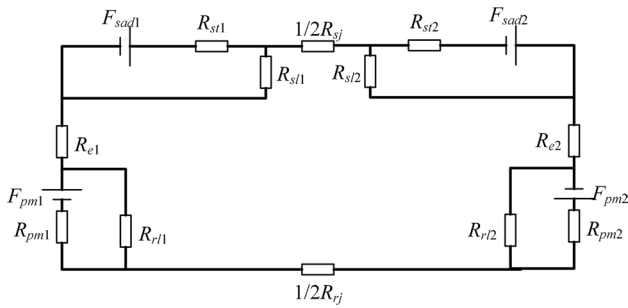
Fig. 3 Equivalent circuit of permanent magnet synchronous motor

Fig. 4 Magnetic density region distribution

R_{e1} and R_{e2} are air gap reluctance; F_{sd1} and F_{sd2} are armature magnetic motive force; R_{sl1} and R_{sl2} are stator side leakage reluctance; R_{st1} and R_{st2} are stator tooth reluctance; R_{sj} is stator yoke reluctance; R_{rj} is rotor yoke reluctance; R_{pm1} and R_{pm2} are permanent magnet reluctance; F_{pm1} and F_{pm2} are permanent magnet magnetic motive force; R_{rl1} and R_{rl2} are rotor side leakage reluctances.

$$\varphi = \frac{2\left(\frac{R_{sl1}}{R_{st1}+R_{sl1}}F_{sd1} + \frac{R_{rl1}}{R_{pm1}+R_{rl1}}F_{pm1}\right)}{2R_{st1} + \frac{R_{sj}}{2} + \frac{R_{rj}}{2} + 2R_{e1} + \frac{2R_{pm1}R_{rl1}}{R_{pm1}+R_{rl1}}} \tag{1}$$

The magnitude of the reluctance is affected by the saturation degree of the magnetic circuit. The formula (1) shows that under the condition of magnetic circuit unsaturation, the main magnetic flux is proportional to the armature magnetic motive force and permanent magnet magnetic motive force. When the magnetic circuit is saturated, the stator yoke reluctance R_{sj} increases gradually with the saturation degree of the magnetic circuit, and the main magnetic flux changes nonlinearly with the armature magnetic motive force and permanent magnet magnetic motive force.
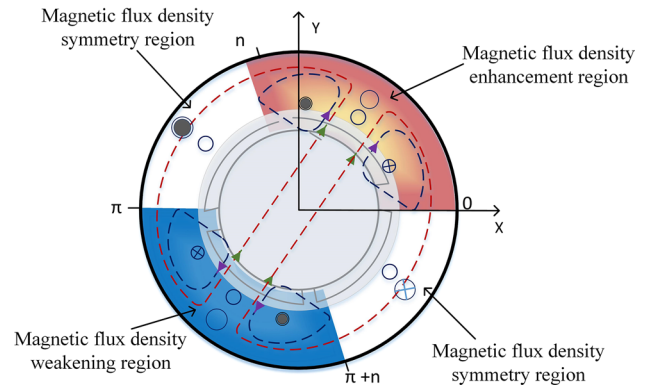
3 The Calculation of Suspension Force Considering The Magnetic Circuit Saturation

In the air gap, the magnetic field is approximately perpendicular to the rotor surface, the tangential magnetic field intensity is approximately 0. The torque magnetic motive force consisted of the magnetic motive force and the permanent magnet magnetic motive force is $f_1(\theta, t)$, and the magnetic motive force of the suspension winding is $f_2(\theta, t)$. According to the maxwell tensor method, the formula of radial suspension force is as follows.

$$\begin{cases} f_1(\theta, t) = F_{1m}\cos(P_1\theta - w_1 t + \varphi_1) \\ f_2(\theta, t) = F_{2m}\cos(P_2\theta - w_2 t + \varphi_2) \\ b_1(\theta, t) = f_1(\theta, t)(\Lambda_0 + \Lambda_1 \cos Z_1\theta) \\ \approx f_1(\theta, t)\Lambda_0 = F_{1m}\Lambda_0 \cos(P_1\theta - w_1 t + \varphi_1) \\ b_2(\theta, t) = f_2(\theta, t)(\Lambda_0 + \Lambda_1 \cos Z_1\theta) \\ \approx f_2(\theta, t)\Lambda_0 = F_{2m}\Lambda_0 \cos(P_2\theta - w_2 t + \varphi_2) \end{cases} \tag{2}$$

$$\begin{aligned} F(\theta,\ t) &= \frac{\mu_{Fe} - \mu_0}{2\mu_{Fe}\mu_0}(B_n^2 + \mu_{Fe}\mu_0 B_t^2)dS \approx \frac{B(\theta,t)^2}{2\mu_0} = \frac{[b_1(\theta,t) + b_2(\theta,t)]^2}{2\mu_0} \\ &= \frac{[F_{1m}\Lambda_0 \cos(P_1\theta - w_1 t + \varphi_1) + F_{2m}\Lambda_0 \cos(P_2\theta - w_2 t + \varphi_2)]^2}{2\mu_0} \end{aligned} \tag{3}$$

where μ_0 is the vacuum permeability, S is the unit surface area of the rotor surface, θ is the space position angle, P_1 is the pole pairs number of the torque magnetomotive force, P_2 is the pole pairs number of the suspension magnetomotive force, b_1 is the torque winding magnetic density, b_2 is the suspension winding magnetic density, w_1 is the angular frequency of torque winding current, w_1 is the angular

suspension force, the stator magnetic circuit is divided into three regions (the magnetic flux density enhancement region, the magnetic flux density weakening region and the magnetic flux density symmetry region) in Fig. 4, which are distributed along the circumference in the range of $0 \sim n$, $n \sim \pi$, $\pi \sim \pi + n$, $\pi + n \sim 2\pi$. The electromagnetic forces of each region are calculated and summed to obtain the radial suspension force.

$$
\begin{aligned}
F_{1x} &= \int_0^n \frac{[b_1(\theta,t)+b_2(\theta,t)]^2 lr\cos\theta}{2\mu_0}d\theta + \int_\pi^{n+\pi} \frac{[b_1(\theta,t)+b_2(\theta,t)]^2 lr\cos\theta}{2\mu_0}d\theta \\
&= \int_0^n \frac{[F_{1m}\Lambda\cos(P_1\theta-w_1t+\varphi_1)+F_{2m}\Lambda\cos(P_2\theta-w_2t+\varphi_2)]^2 lr\cos\theta}{2\mu_0}d\theta \\
&+ \int_\pi^{n+\pi} \frac{[F_{1m}\Lambda\cos(P_1\theta-w_1t+\varphi_1)+F_{2m}\Lambda\cos(P_2\theta-w_2t+\varphi_2)]^2 lr\cos\theta}{2\mu_0}d\theta
\end{aligned}
\tag{4}
$$

$$
\begin{aligned}
F_{2x} &= \int_n^\pi \frac{[b_1(\theta,t)+b_2(\theta,t)]^2 lr\cos\theta}{2\mu_0}d\theta + \int_{n+\pi}^{2\pi} \frac{[b_1(\theta,t)+b_2(\theta,t)]^2 lr\cos\theta}{2\mu_0}d\theta \\
&= \int_n^\pi \frac{[F_{1m}\Lambda\cos(P_1\theta-w_1t+\varphi_1)+F_{2m}\Lambda\cos(P_2\theta-w_2t+\varphi_2)]^2 lr\cos\theta}{2\mu_0}d\theta \\
&+ \int_{n+\pi}^{2\pi} \frac{[F_{1m}\Lambda\cos(P_1\theta-w_1t+\varphi_1)+F_{2m}\Lambda\cos(P_2\theta-w_2t+\varphi_2)]^2 lr\cos\theta}{2\mu_0}d\theta \\
&= 0
\end{aligned}
\tag{5}
$$

$$
\begin{aligned}
F &= F_{1x} + F_{2x} \\
&= \frac{lr(\Lambda_1^2+\Lambda_2^2)F_{1m}F_{2m}}{2}\left[n\cos(\varphi_1-\varphi_2)+\frac{1}{2}\sin(2n-\varphi_1+\varphi_2)+\frac{1}{2}\sin(\varphi_1-\varphi_2)\right] \\
&+ \frac{lr(\Lambda_1^2-\Lambda_2^2)F_{1m}F_{2m}}{2(P_1+P_2\pm 1)}\left[\sin\left[(P_1+P_2\pm 1)n-2w_1t-(\varphi_1+\varphi_2)\right]+\sin(2w_1t+\varphi_1+\varphi_2)\right] \\
&+ \frac{lr(\Lambda_1^2-\Lambda_2^2)F_{1m}^2}{42P_2\pm 1}\sin\left[(2P_1-1)n-2w_1t-2\varphi_1\right] \\
&+ \frac{lr(\Lambda_1^2-\Lambda_2^2)F_{2m}^2}{42P_2\pm 1}\sin\left[(2P_2-1)n-2w_2t-2\varphi_2\right]
\end{aligned}
\tag{6}
$$

frequency of suspension winding current, φ is the initial phase angle, Λ_0 is the invariant part of the air gap permeability, Λ_1 is the teeth harmonic magnetic permeability.

From the above equations, the magnitude of the radial suspension force is related to the magnetic motive force and magnetic permeability. Influenced by the properties of ferromagnetic materials, when the magnetic circuit is saturated, the permeability decreases nonlinearly with the increase of magnetic density. The coupling of the 4-pole magnetic field and the 2-pole magnetic field increases the possibility of magnetic circuit saturation. In order to accurately calculate the radial

L is the motor axial direction, r is the rotor outer diameter, Λ_1 is the average magnetic permeability of the magnetic density enhancement region, Λ_2 is the average magnetic permeability of the magnetic density weakening region, θ is the space position angle. From the above analytical formula, it can be seen that the suspension force is consisted of the stable component ① and the fluctuating components ②, ③ and ④ The magnitude of suspension force is related to the magnetic motive force and the magnetic permeability. In the situation of magnetic circuit unsaturation, the magnetic permeability of the enhancement region and the weakening region are

Table 1 Parameters of the prototype

Parameters	Value	Unit
Power	8.5	kW
Axial length of motor	72	mm
Rotation speed	4000	r/min
Outer diameter of stator	180	mm
Inner diameter of stator	103	mm
Outer diameter of rotor	96.4	mm
Thikness of permanent motor	3.18	mm
Number of stator slots	36	
Number of parallel branches	1	
Permanent magnet material	N35SH	
Permanent magnet magnetization method	Radial magnetization	
Number of turns of torque winding	24	
Number of turns of suspension winding	22	
Number of torque winding pole pairs	2	
Number of suspension winding pole pairs	1	

Fig. 5 The bearingless permanent magnet synchronous motor winding arrangement

approximately the same ($\Lambda_1 \approx \Lambda_2$). The magnitude of the stable component of suspension force is proportional to the magnetic motive force, and the magnitude of the fluctuating component of suspension force is approximately 0. When the magnetic circuit of the enhancement region is saturated, the magnetic permeability will change, which is not the same as that in the weakening region ($\Lambda_1 \approx \Lambda_2$). The variation of magnetic permeability will further cause the change of suspension performance.

The increase of the torque magnetic motive force or the suspension magnetic motive force will cause the saturation of the magnetic circuit, and the magnetic permeability of the saturation region will decrease nonlinearly with the increase of the magnetic motive force. In the case of saturation, the magnetic motive force F_{1m} (or F_{2m}) increases, the magnetic permeability $\Lambda_1^2 + \Lambda_2^2$ decreases. When the increase of the magnetic motive force is greater than the decrease of the magnetic permeability, the stable component of the suspension force will increase nonlinearly with the increase of the magnetic motive force. When the increase of magnetic motive force is smaller than the decrease of magnetic permeability, the stable component of the suspension force will decrease nonlinearly with the increase of magnetic motive force. When the magnetic circuit is saturated, the magnetic permeability $\Lambda_1^2 - \Lambda_2^2$ will increase with the increase of magnetic motive force. The fluctuation component of the suspension force will increase nonlinearly with the increase of the magnetic motive force, which cause the fluctuation of suspension force. So, the magnetic circuit saturation will affect the stability of the suspension force, and the stability of the suspension force becomes worse with the increase of saturation degree.
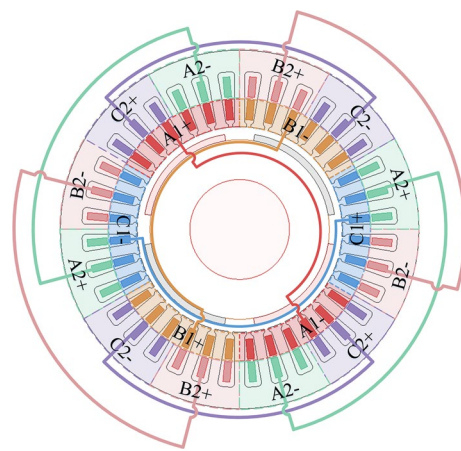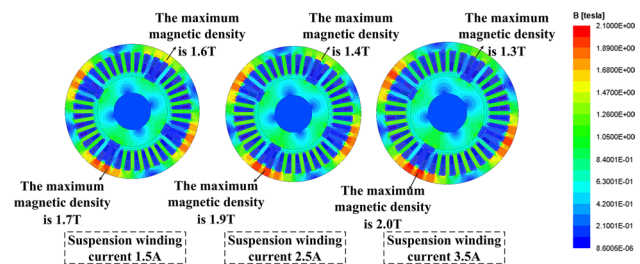

Fig. 6 The magnetic density distribution with the increase of suspension magnetic
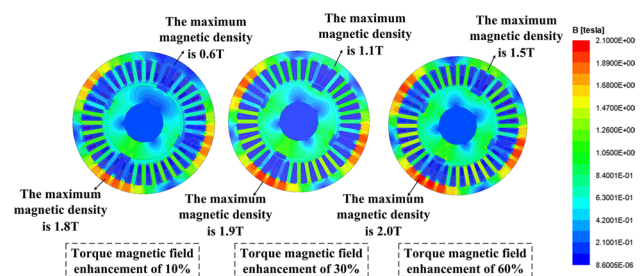

Fig. 7 The magnetic density distribution with the increase of torque magnetic field

4 Effect of Magnetic Circuit Saturation on Suspension Force

4.1 Analysis of Magnetic Field Distribution Characteristics under Different Saturation Conditions of The Magnetic Circuit

To further clarify the effect of magnetic circuit saturation on the suspension performance, the mathematical model is

established based on the finite element method. The parameters are shown in Table 1. The arrangement of the torque and suspension windings is given in Fig. 5. A1, B1 and C1 are the suspension windings and A2, B2 and C2 are the torque windings.

The saturation of the magnetic circuit is closely related to the torque magnetic field and the suspension magnetic. In order to clarify the effect of the magnitude of the torque magnetic field and the suspension magnetic field on the magnetic circuit saturation. The magnetic field distribution under different conditions of magnetic circuit saturation is calculated. The variation of the magnetic density distribution with the increase of suspension magnetic field and the torque magnetic field are shown in Figs. 6 and 7.

The variation of the magnetic density distribution with the increase of suspension magnetic field is shown in Fig. 6. As the suspension winding current increases from 1 to 5A, the magnetic density of the enhancement region increases from 1.7 T to 2.0 T, and the magnetic density of the weakening region decreases from 1.7 T to 0.6 T. The variation of the magnetic density distribution with the increase of torque magnetic field is shown in Fig. 7. When the torque magnetic field increases, the magnetic density increases in both regions.

The above analysis shows that the variation characteristic of magnetic density distribution with the increase of coupled magnetic field is different. As the torque field increases, the two regions will be saturated. While with the suspension field increase, only the magnetic density enhancement region will be saturated.

4.2 Analysis of Suspension Performance at Different Saturation States

The magnetic circuit saturation will affect the suspension performance of the motor. In order to explore the change of suspension force under different saturation states, the magnitude and fluctuation of suspension force is calculated in the case of magnetic circuit saturation caused by torque magnetic field and suspension magnetic field separately. Figure 8 gives the variation of the magnitude and fluctuation of the suspension force with the increase of suspension magnetic field.

The magnitude of the suspension magnetic field increases gradually with the increase of suspension winding current. It can be seen from Fig. 8 that when the suspension winding current is less than 3A, the magnitude of the suspension force is proportional to the magnitude of the suspension magnetic field. The suspension force magnitude increases by 107N when the suspension winding current changes from 1 to 3A. When the suspension winding current is larger than 3A, the magnitude of the suspension force increases nonlinearly with the increase of suspension magnetic field. The suspension force increases by only 50N when the suspension winding current changes from 6 to 8A.

When the suspension current is less than 3A, the fluctuation of suspension force accounts for 4.38% of the suspension force. The fluctuation of suspension force gradually increases when the suspension winding current is larger than 3A. When the suspension winding current
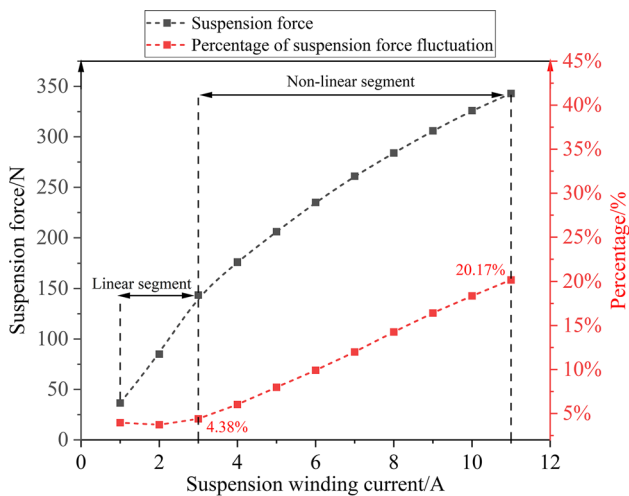

Fig. 8 Variation of the magnitude and fluctuation of the suspension force with the suspension magnetic field
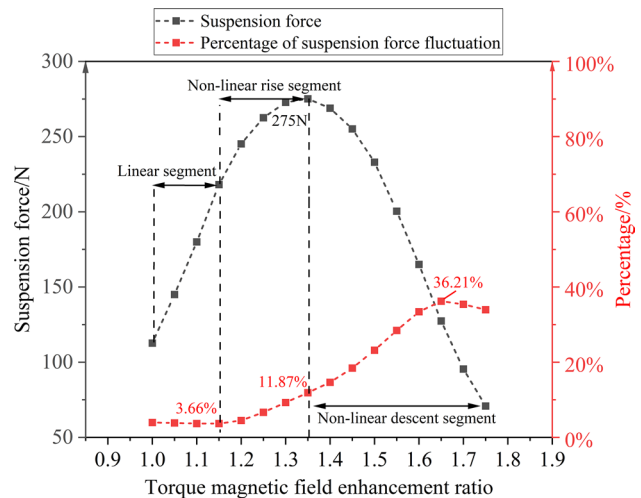

Fig. 9 Variation of the magnitude and fluctuation of the suspension force with the torque magnetic field

is 11A, the fluctuation of suspension force accounts for 20.17% of the suspension force, which is 5 times that the suspension winding current being 3A.

The Fig. 9 gives the variation of the magnitude and fluctuation of the suspension force with the increase of torque magnetic field. When the increase of the torque magnetic field is less than 15%, the magnitude of the suspension force will increase linearly with the increase of torque magnetic field. The magnitude of suspension force increases by 106N when the torque magnetic field increases by 15%. When the torque magnetic field increases more than 15%, the suspension force first increases and then decreases. When the torque magnetic field is increased by 35%, the magnitude of the suspension is the largest, which is 275 N.

The fluctuation of suspension force accounts for 3.66% of the suspension force when the increase of the torque magnetic field is less than 15%. After the increase of torque magnetic field exceeding 15%, the fluctuation of suspension force sharply increases with the increase of torque magnetic field. The fluctuation of the suspension force accounts for 36.21% of the suspension force when the torque magnetic field increases by 70%, which is 9 times higher than the torque magnetic field increasing by 15%.

4.3 The Relationship Analysis of The Magnitude and Phase of Suspension Force

Because the rotor of bearingless motor may have radial displacement during operation, the direction of suspension force needs to be constantly adjusted to make the motor work stably. The saturation of the magnetic circuit will
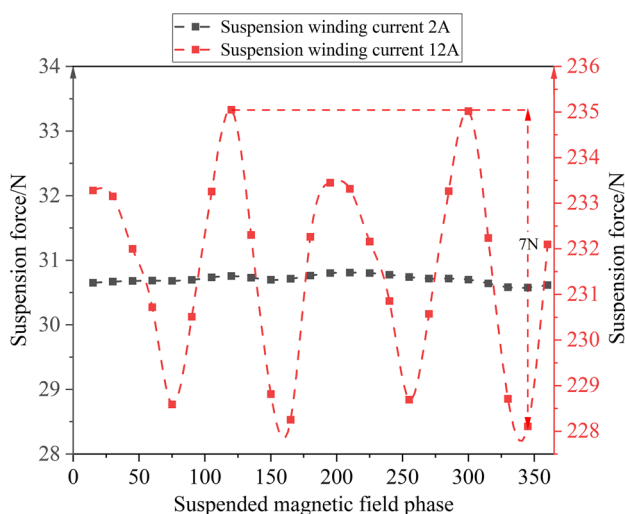
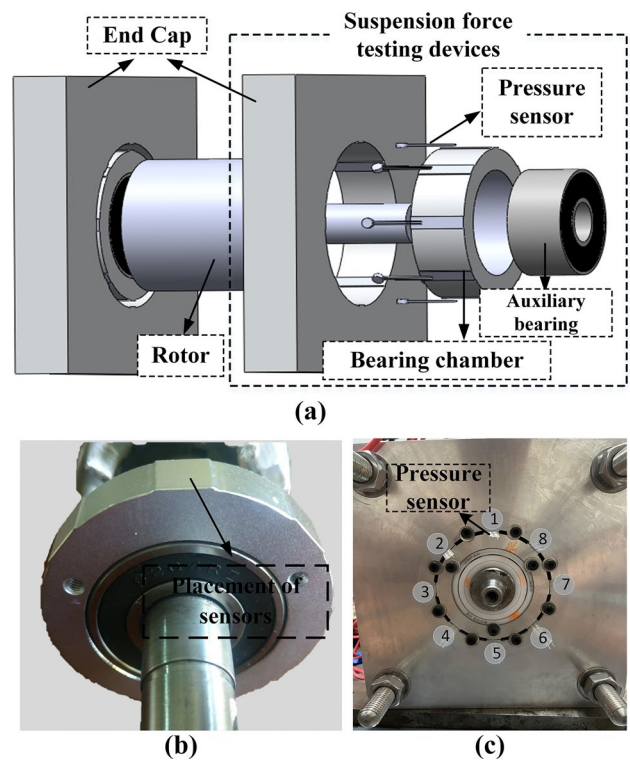**Fig. 10** The suspension force under different suspension magnetic field phases

Fig. 11 The measurement diagram of suspension force

affect magnitude of the suspension force when the suspension magnetic field phase is adjusted. In order to study the influence of magnetic circuit saturation on the relationship between the magnetic field phase and the suspension force magnitude, the magnitude of suspension force under different magnetic field phases is calculated.

As can be seen from Fig. 10, the magnitude of the suspension force is the same at different suspension magnetic field phases when magnetic circuit is unsaturated, and the variation of the suspension force magnitude is 0.2N at most. However, when magnetic circuit is saturated, the magnitude of the suspension force is different at different suspension magnetic field phases, and the variation of the suspension force magnitude is 7N at most. Therefore, in the process of magnetic field regulation, it is necessary to consider the influence of magnetic circuit saturation on the suspension force.

5 Experimental Verification

In order to further verify the effective and accuracy of the theoretical analysis and numerical calculation, an experimental prototype is made and tested. As shown in Fig. 11, the suspension force testing mechanism is placed at the end covers. The pressure sensors for measuring the radial suspension force are placed between the bearing chamber
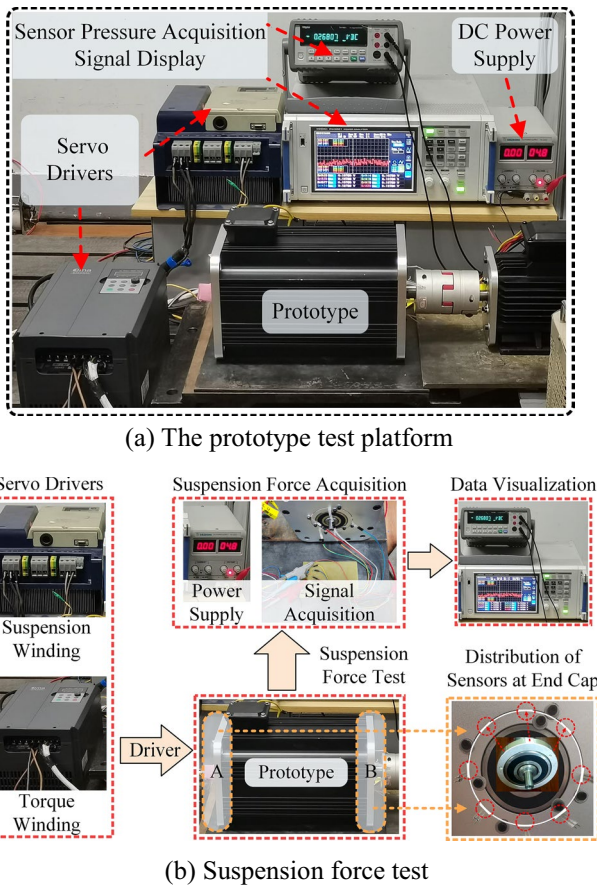
(a) The prototype test platform

(b) Suspension force test

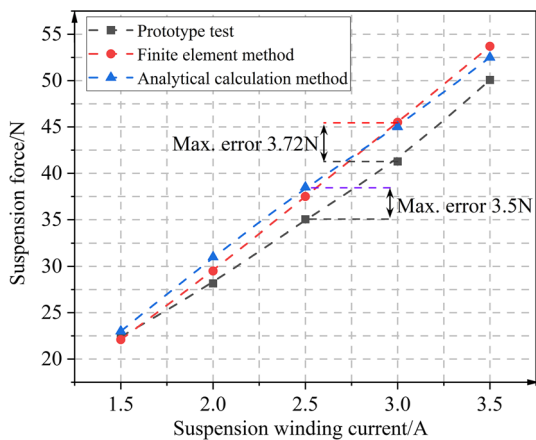**Fig. 12** Experimental prototype of BPMSM

Fig. 13 The results comparison of experimental, finite element calculation and analytical calculation

and bearing, and eight pressure sensors are placed around the circumference of the bearing chamber to ensure the accuracy of the suspension force testing.

The prototype is placed on the test bench shown in Fig. 12(a). The experimental equipment mainly includes transformer, bearingless permanent magnet synchronous motor, power analyzer, voltage signal acquisition circuit, etc. Figure 12(b) shows the suspension force test. When the prototype is operated, the pressure signal is collected through the sensors at the end caps of the motor and the signal acquisition circuit. The collected signals are displayed by the oscilloscope.

1) Static suspension test: In order to verify the influence of the magnetic motive force of the suspension winding on the suspension performance, the static test method is used to test the values of each sensor when the current of the suspension winding are different, and the magnitude of the suspension force is obtained by the vector synthesis. The experimental results, finite element calculation results and analytical calculation results are given in Fig. 13, respectively.

It can be seen from the Fig. 13 that the value of the suspension force texted by experiment increases with the increase of the suspension winding current, which is consistent with the results of the finite element calculation and the analytical calculation, and the maximum error is 3.62N(9%) and 3.5N(10%), respectively.

2) Dynamic suspension test: In order to investigate the influence of winding frequency on suspension performance, the values of each sensor under different winding frequencies are tested. The experimental values of the suspension force are obtained by mathematical analysis, as shown in Table 2.

As can be seen from Table 2, with the increase of frequency, the magnitude of the suspension force remains constant. When the frequency of the motor is changed from 20 to 50 Hz, the prototype test results are around 28N, the results of analytical calculation and finite element calculation are around 31.4N and 27.3N, respectively. The maximum relative error of the suspension force between the finite element calculation and the prototype test is 2.2N (7.9%). And the maximum relative error between the analytical calculation results and the prototype test is 3.8N (13.6%).

Table 2 Dynamic suspension force measurement results

Frequency (A)	Test results (N)	FEM results (N)	Analytical results (N)
20	26.2	28.4	31.1
30	28.4	27.6	31.3
40	28.3	27.7	31.5
50	27.7	28.4	31.7

6 Conclusion

In this paper, a nonlinear mathematical model of the suspension force considering the magnetic circuit saturation is proposed. Based on finite element method, the magnitude and fluctuation of suspension force are calculated and analyzed. Combined with finite element analysis, the following conclusions are drawn:

1) The distribution characteristics of magnetic field in the case of magnetic circuit saturation caused by torque magnetic field are different from that caused by suspension magnetic field. With the increase of the suspension magnetic field, the magnetic density of enhancement region increases from 1.7 T to 2.0 T, and the magnetic density of the magnetic density weakening region decrease from 1.7 T to 0.6 T. While, with the increase of the torque magnetic field, the magnetic density of the two regions both increase by 0.4 T.

2) Affected by the magnetic circuit saturation, the suspension force will nonlinearly increases with the increase of coupled magnetic field. The magnitude of the suspension force increases by 107N when the suspension winding current changes from 1 to 3A, while the suspension force increases by only 50N when the suspension winding current changes from 6 to 8A. As the torque magnetic field increase, the magnitude of the suspension force first increases and then decreases. The suspension force reaches a maximum of 275N when the torque magnet magnetic field increase by 35%.

3) Compared to the unsaturated case, magnetic circuit saturation will cause sharp increase of suspension force fluctuation. When the suspension winding current increases from 3 to 11A, the fluctuation of suspension force increases from 4 to 20%. When the torque magnetic field increases from 15 to 50%, the fluctuation of suspension force increases from 3.6% to 20%.

4) Affected by the magnetic circuit saturation, in the process of adjusting the phase of suspension magnetic field, the magnitude of the suspension force will change. When the magnetic circuit is unsaturated, the magnitude of the suspension force is the same under the different phases of suspension magnetic field, and the variation of suspension force is 0.2N at most. When the magnetic circuit is saturated, the magnitude of the suspension force is different, and the variation of suspension force is 7N at most.

Declarations

Conflict of interest No potential conflict of interest was reported by the authors.

References

1. Pei T, Li D, Liu J, Li J, Kong W (2022) Review of bearingless synchronous motors: principle and topology. IEEE Trans Transp Electr 8(3):34893502
2. Chen J, Zhu J, Severson EL (2020) Review of bearingless motor technology for significant power applications. IEEE Trans Indust Appl 56(2):1377–1388
3. Hemenway NR, Gjemdal H, Severson EL (2021) New three-pole combined radial-axial magnetic bearing for industrial bearingless motor systems. IEEE Trans Indust Appl 57(6):6754–6764
4. Puentener P, Schuck M, Kolar JW (2020) The influence of impeller geometries on hemolysis in bearingless centrifugal pumps. IEEE Open J Eng Med Biol 1:316–323
5. Bartholet MT, Nussbaumer T, Silber S, Kolar JW (2009) "Comparative evaluation of polyphase bearingless slice motors for fluid-handling applications. In IEEE Trans Indust Appl 45(5):1821–1830
6. Chen J, Zhu J, Severson EL (2020) Review of bearingless motor technology for significant power applications. IEEE Trans Indust Appl 56(2):1377–1388
7. Wang F, Zhu Y, Wang H, Zhao D (2020) Design and analysis of a bearingless permanent-magnet motor for axial blood pump applications. IEEE Access 8:7622–7627
8. Kurita N, Ishikawa T, Saito N, Masuzawa T, Timms DL (2019) A dual-sided stator type axial bearingless motor development for total artificial heart. IEEE Trans Indust Appl 55(2):1516–1523
9. Cui Z, Zhou Y, Zhang J, Liu W (2022) Modeling and analysis of dual-winding bearingless flux-switching permanent magnet motor considering magnetic saturation based on subdomain model. IEEE Trans Energy Convers 37(1):132–144
10. Takemoto M, Chiba A, Akagi H, Fukao T (2004) Radial force and torque of a bearingless switched reluctance motor operating in a region of magnetic saturation. IEEE Trans Indust Appl 40(1):103–112
11. Wang Z, Cao X, Deng Z, Cai J and Deng X (2022) Electromagnetic modeling and investigation for bearingless switched reluctance motor considering magnetic saturation. In IEEE transactions on energy conversion.
12. Zhu Z, Zhu H, Li X, Zhu J, Cheng M (2021) Dynamic equivalent magnetic network analysis of an axial PM bearingless flywheel machine. IEEE Access 9:32425–32435
13. Wang Z, Cao X and Deng Z (2021) Nonlinear torque modeling for bearingless switched reluctance motor considering magnetic saturation. 2021 IEEE 30th international symposium on industrial electronics (ISIE), pp 1–6.
14. Shi Z, Sun X, Lei G, Tian X, Guo Y, Zhu J (Oct.2022) Multiobjective optimization of a five-phase bearingless permanent magnet motor considering winding area. IEEE/ASME Trans Mechatron 27(5):2657–2666
15. Sun X, Jin Z, Cai Y, Yang Z, Chen L (2020) Grey wolf optimization algorithm based state feedback control for a bearingless permanent magnet synchronous machine. IEEE Trans Power Electron 35(12):13631–13640

Liming Liu He is working toward the M.S. degree in electrical machines at Zhengzhou University of Light Industry. His current research interests include electromagnetic and thermal analysis on electrical machines, particularly on high speed permanent magnetic machines.

Hongbo Qiu Hereceived the M.S. degree inelectrical engineering from theHarbin University of Scienceand Technology, Harbin, China,in 2012, and the Ph.D. degreein electrical engineering fromthe Harbin University ofScience and Technology, in2014. He has been with theZhengzhou University of Light Industry, Zhengzhou, China,since 2014. His research interests include electromagneticand thermal analysis on electrical machine, especially inpermanent magnetic machines.